Tailoring local acid-like microenvironment with the synergism of nano and atomic electric fields for enhanced hydrogen spillover in alkaline seawater electrolysis

Lei Jin, Zhiyuan Wang, Hui Xu*, Kun Wang, Xingyue Qian, Haiqun Chen*, Guangyu He*

Key Laboratory of Advanced Catalytic Materials and Technology, Advanced Catalysis and Green Manufacturing Collaborative Innovation Center, Changzhou University, Changzhou, Jiangsu Province 213164, China

Corresponding authors: xuhui006@cczu.edu.cn (H. Xu); chenhq@cczu.edu.cn (H. Chen); hegy@cczu.edu.cn (G. He)

1. Material Characterizations

The crystal phases and structures of the as-prepared samples were characterized by powder X-ray diffraction (XRD) with Bruker D8 Advance diffractometer (Cu Ka radiation, $\lambda = 0.15418$ nm) in the 2θ range of 20-80° at a scanning rate of 0.05° s^{-1}. The microstructures of the products were observed by transmission electron microscopy (TEM, JEM-2100F) and field-emission scanning electron microscopy (FESEM, Zeiss Supra 55) that equipped with element mappings. The morphologies of the materials were characterized by scanning electron microscopy (SEM, Zeiss Sigma 300 Cold Field scanning electron microscope). X-ray photoelectron spectroscopy (XPS, PHI-5000C ESCA, PerkinElmer, USA) was employed to obtain elemental information of prepared catalysts on a VG ESCALAB MKII using Al Ka radiation. Ultraviolet photoelectron spectroscopy (UPS) is performed on Thermo ESCALAB Xi+ equipped with ultraviolet photoelectron spectrometer (Hel (21.22 eV)). In Situ Raman Measurement: In situ Raman spectra were recorded on XpoloRA PLUS Raman spectrometer with 532 nm wavenumber of the excitation light source. Electron paramagnetic resonance (EPR) spectra were recorded on a Bruker EPR ELEXSYS 500 spectrometer. The Fourier transform infrared spectrometer (FT-IR, Nicolet iS5) was recorded to detect the functional groups of samples in the range of 200-4000 cm^{-1}. Inductively coupled plasma optical emission spectroscopy (ICP-OES) characterization was performed on an Agilent Varian 720ES equipment.

2. Electrochemical Measurements

All the electrochemical measurements were tested using a CHI760E electrochemical workstation with a standard three electrode cell. The reference electrodes were Hg/HgO or Ag/AgCl in alkaline or acidic solution, respectively, the counter electrode was graphite rod. A glassy carbon electrode (GCE. 5 mm inner diameter, 0.196 cm^2 area) that modified with catalyst ink is used as the working electrode. The homogeneous catalyst ink was made by ultrasonically dispersing a mixture containing 2 mg of catalyst, 20 μL Nafion (5 wt%), 360 μL ethanol and 120 μL H_2O. Then, 10 μL of the catalyst ink was dropped on the surface of GCE with an approximate mass loading of 203.8 $μg·cm^{-2}$. Taking the alkaline test as an example, all

potentials were measured against Hg/HgO or Ag/AgCl, and converted to reversible hydrogen electrode (RHE) by Nernst equation: $E_{vs\,RHE} = E_{vs\,Hg/HgO} + 0.0591 \cdot pH + 0.098$. The overpotential (η) was calculated through the formula: $\eta = E_{RHE}$. Cyclic Voltammograms (CV) were measured at a scan rate of 5 $mV \cdot s^{-1}$. Electrochemical impedance spectroscopy was tested over the frequency range of 10^6 to 10^{-2} Hz with an AC signal amplitude of 5 mV. The double-layer capacitance (C_{dl}) was evaluated by cyclic voltammetry (CV) curves performed at the non-faraday reaction regions with an interval of 20 $mV \cdot s^{-1}$ over the scanning range of 20 ~ 120 $mV \cdot s^{-1}$. The turnover frequency (TOF) values were calculated from the following equation: TOF (s^{-1}) = (j × A)/ (k × F × n). Here, k is the number of electron transfer (the factors of HER is 2), j is the current density at a given overpotential, A is the geometric surface area of the electrode, F is the Faraday constant (96485.3 C mol^{-1}), n is the number of active sites (mol). The number of voltammetric charges is gained by CV curves from 0 ~ 0.6 V *vs*. RHE for HER in a phosphate buffer solution (pH ~ 7) with a scan rate of 50 mV s^{-1} respectively, and the following equation is n (mol) = Q/2F (the surface charge Q is proportional to the number of active sites). The long-term stability of the catalyst was conducted by chronopotentiometry (CP). All the data of electrochemistry were presented without any i*R* correction.

3. Finite Element Simulations

Free electron density and electric field around electrode were simulated using the COMSOL multiphysics finite-element-based solver[1]. The "electrostatics" module was used to simulate electric field when the electrode is under a specific potential bias. The electric field, E, was computed as the negative gradient of the electric potential as follows:

$$E = -\nabla V$$

The simulation model for Ru nanoparticles was regarded as nanospheres with a diameter of about 150 nm. The electric potentials 1 V was applied to the bottom of the high-curvature nanoparticles.

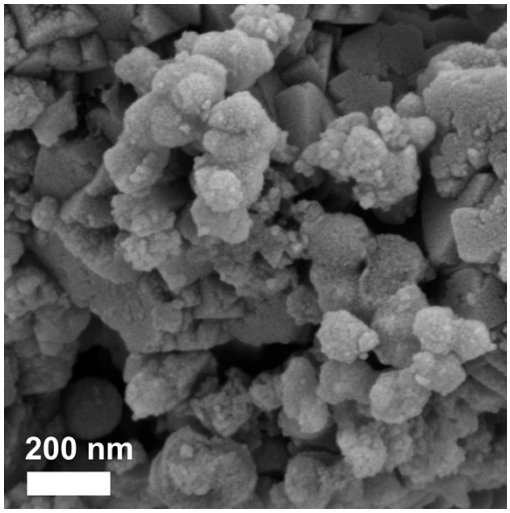

Fig. S1 SEM image of the Ru-$Co(OH)_2$.

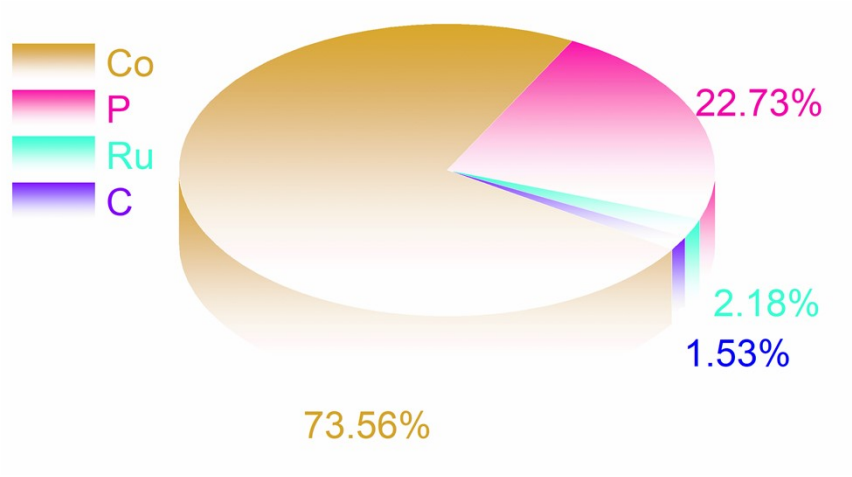

Fig.S2 The content of element in Ru-Co_xPv@C catalyst

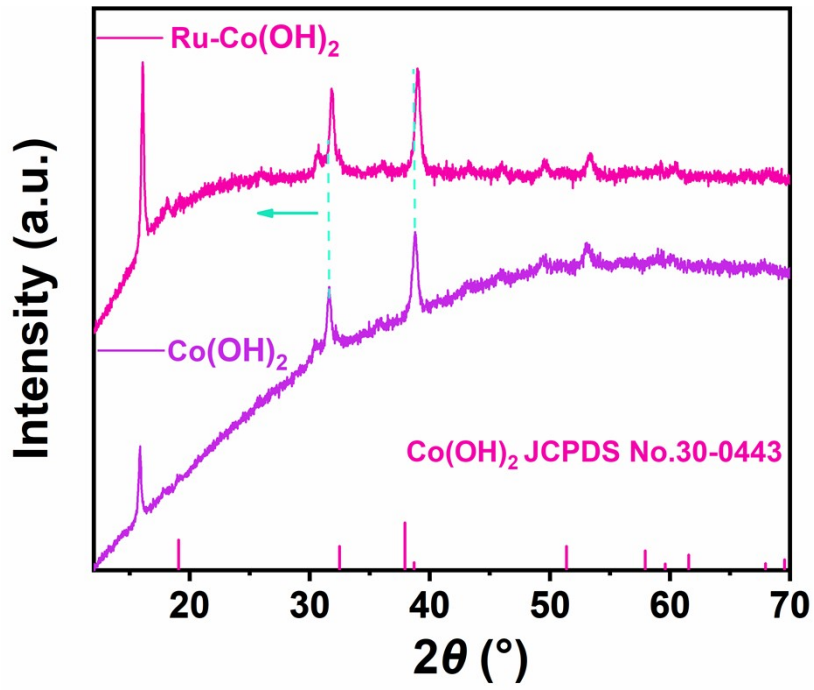

Fig. S3 XRD pattern of the $Co(OH)_2$ and Ru-$Co(OH)_2$.

Table S1. UPS measured work functions of as-prepared catalysts

Catalysts	E_{cutoff} (eV)	ΔE (eV)	Φ (eV)
Co_xP	15.27	4.02	5.95
$Co(OH)_2$	15.05	1.94	6.17
Ru	-----	-----	6

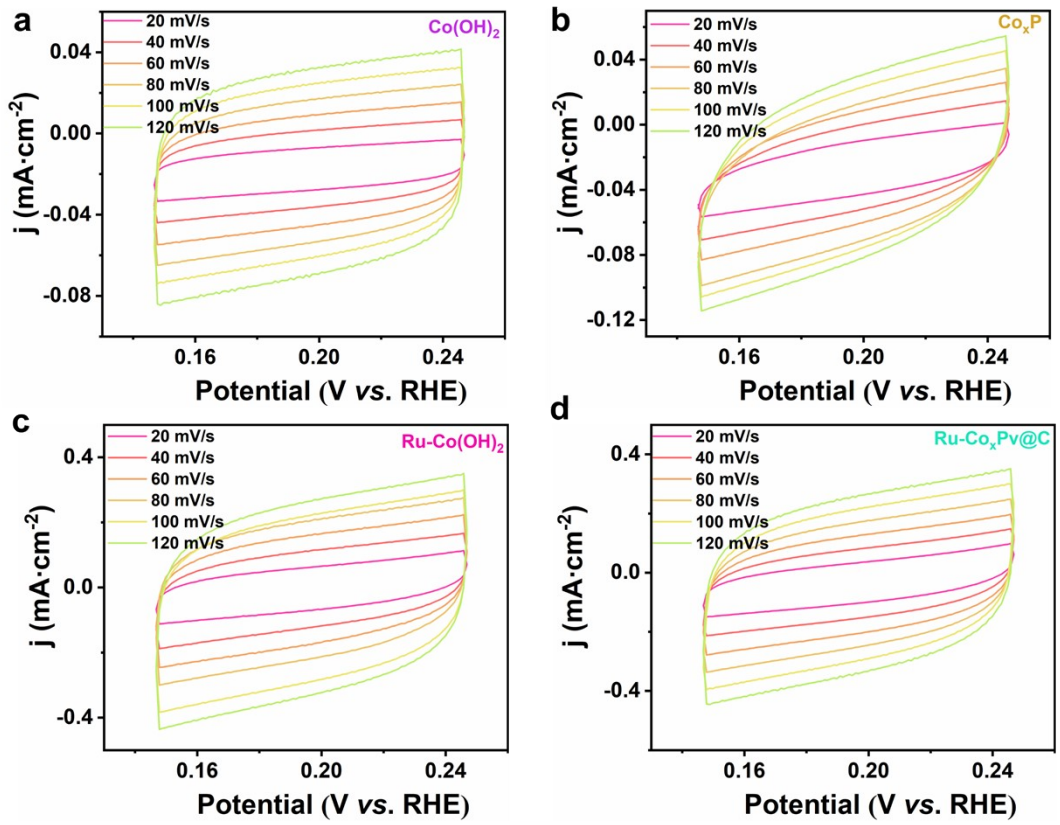

Fig. S4 (a-d) CV curves of different electrocatalysts with different scanning rates for HER in alkaline seawater solution.

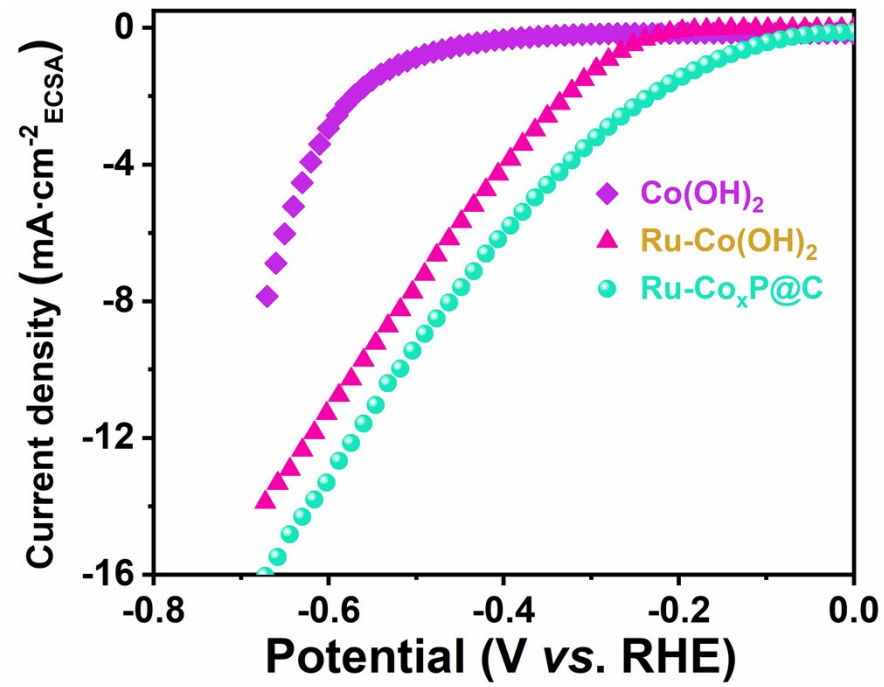

Fig. S5 LSV curves normalized to the ECSA.

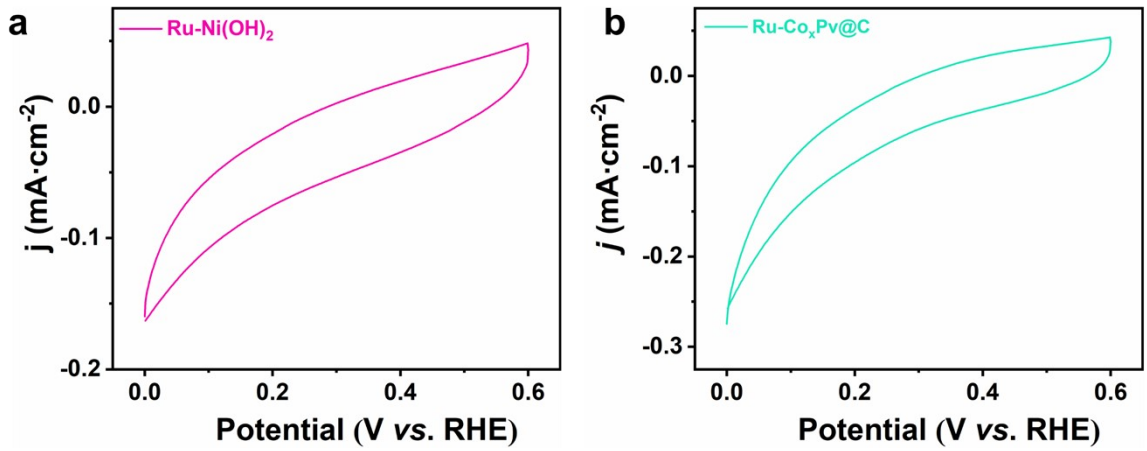

Fig. S6 (a, b) CV curves from 0 to 0.6 V *vs.* RHE for HER in 1.0 M PBS (pH = 7) at 50 mV s^{-1}).

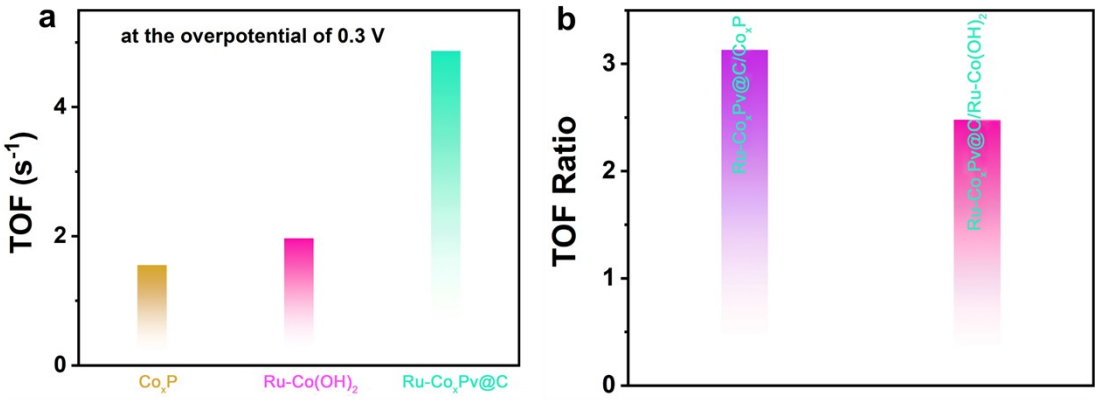

Fig. S7 (a) TOF values and (b) TOF ratio of catalysts.

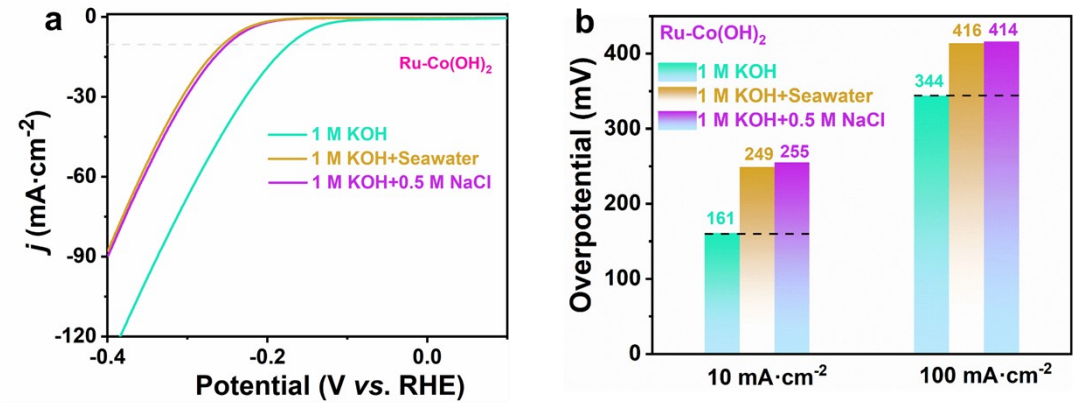

Fig. S8 (a) LSVcurves of Ru-Co(OH)$_2$ in various solutions and (b) corresponding overpotential of at 10 and 100 mA·cm^{-2}.

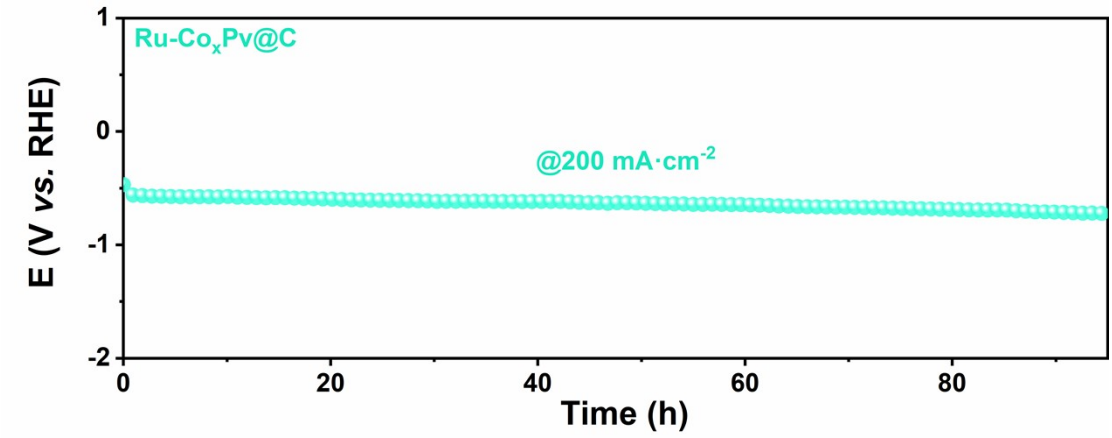

Fig. S9 CP curves of Ru-Co$_x$Pv@C at 200 mA·cm^{-2}

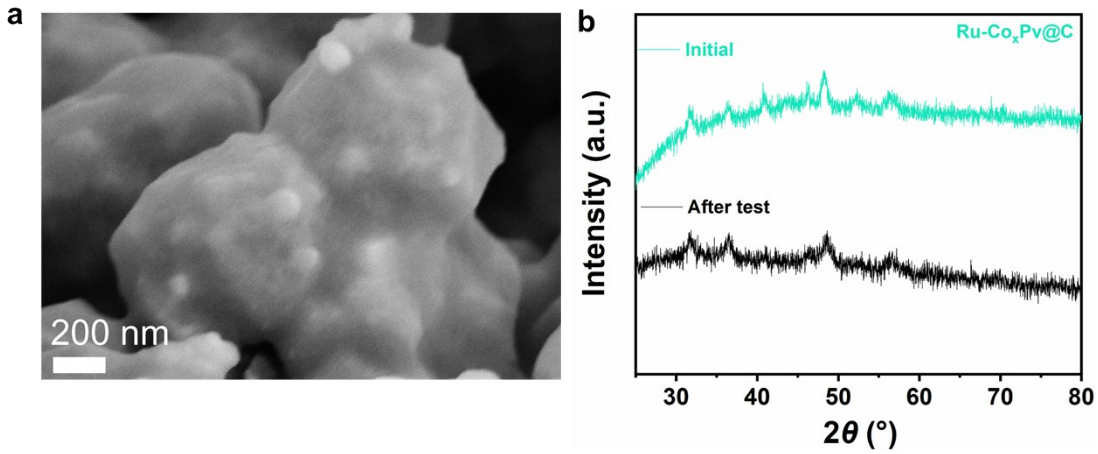

Fig. S10 (a) Sem of Ru-Co$_x$Pv@C after prolonged electrolysis, (b) XRD of Ru-Co$_x$Pv@C before and after prolonged electrolysis.

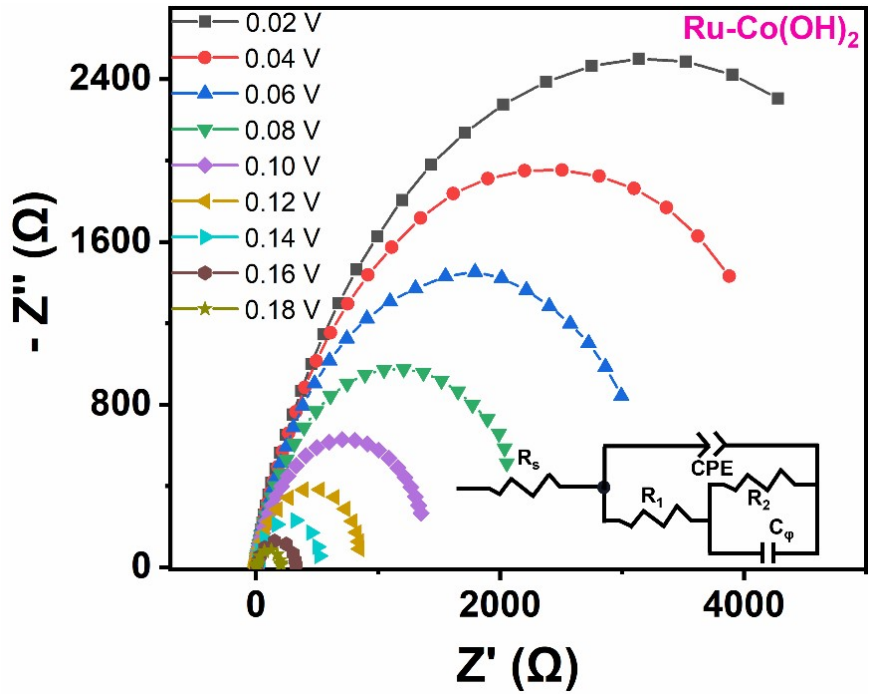

Fig. S11 EIS curves of Ru-$Co(OH)_2$ for HER in alkaline seawater solution.

Table S2 The alkaline OWS performance of Ru-Co_xPv@C with some representative bifunctional electrocatalysts reported.

Catalysts	Electrolyte	Voltage (V)	Ref.
Ru-Co_xPv@C	**1.0 KOH+ seawater**	**1.58**	**This work**
CoNSC	1.0 KOH	1.64	2
CoP@NCNHP	1.0 KOH	1.64	3
CoP@SNC	1.0 KOH	1.64	4
v-NiS_2/CeO_2	1.0 KOH	1.64	5
$NiCo_2O_4$	1.0 KOH	1.65	6
Co-NC/CF	1.0 KOH	1.67	7
NiFe LDH/NF	1.0 KOH	1.7	8
Ni_5P_4/NF	1.0 KOH	1.7	9
Ni_3S_2	1.0 KOH	1.76	10

Table S3 The fitted parameters of the EIS data of Ru-$Co(OH)_2$ and Ru-Co_xPv@C for HER in alkaline seawater.

Catalysis	η (mV)	Rs (Ω)	R_1 (Ω)	R_2 (Ω)	$C_φ$ (μF)
	-20	9.025	15.64	608.7	106.51
	-40	9.115	14.5	311.9	123.33
	-60	8.983	11.45	173.1	125.59
Ru-	-80	8.891	9.823	105.3	134.55
Co_xPv@C	-100	8.869	8.858	71.33	138.22
	-120	9.146	7.37	49.07	143.65
	-140	8.596	6.89	35.87	144.27
	-160	8.722	6.368	26.53	145.34
	-180	8.791	6.191	20.12	147.52
	-20	3.728	309.9	5693	0.3564
	-40	3.683	238.9	4428	0.53984
	-60	3.624	197.8	3075	0.59759
	-80	3.596	184.7	2118	0.8397
Ru-$Co(OH)_2$	-100	3.574	27.79	1440	2.6931
	-120	3.585	33.95	860	3.4708
	-140	3.624	27.75	514.1	6.0847
	-160	3.618	26.64	309	8.4029
	-180	3.6	20.77	190.7	12.271

References

1. F. Xue, C. Zhang, H. Peng, F. Liu, X. Yan, Q. Yao, Z. Hu, T.-S. Chan, M. Liu, J. Zhang, Nanotip-induced electric field for hydrogen catalysis, Nano Lett., 2023, **23**, 11827-11834.

2. Z. Zhang, X. Zhao, S. Xi, L. Zhang, Z. Chen, Z. Zeng, M. Huang, H. Yang, B. Liu, S.J. Pennycook, Atomically dispersed cobalt trifunctional electrocatalysts with tailored coordination environment for flexible rechargeable Zn-air battery and self-driven water splitting, Adv. Energy Mater., 2020, **10**, 2002896.

3. Y. Pan, K. Sun, S. Liu, X. Cao, K. Wu, W.-C. Cheong, Z. Chen, Y. Wang, Y. Li, Y. Liu, Core-shell ZIF-8@ ZIF-67-derived CoP nanoparticle-embedded N-doped carbon nanotube hollow polyhedron for efficient overall water splitting, J. Am. Chem. Soc., 2018, **140** 2610-2618.

4. T. Meng, Y.-N. Hao, L. Zheng, M. Cao, Organophosphoric acid-derived CoP quantum dots@S, N-codoped graphite carbon as a trifunctional electrocatalyst for overall water splitting and Zn-air batteries, Nanoscale, 2018, **10**, 14613-14626.

5. W. Liao, W. Li, Y. Zhang, Sulfur and oxygen dual vacancies manipulation on 2D NiS_2/CeO_2 hybrid heterostructure to boost overall water splitting activity, Mater. Today Chem., 2022, **24**, 100791.

6. X. Gao, H. Zhang, Q. Li, X. Yu, Z. Hong, X. Zhang, C. Liang, Z. Lin, Hierarchical $NiCo_2O_4$ hollow microcuboids as bifunctional electrocatalysts for overall water-splitting, Angew. Chem. Int. Ed., 2016, **55**, 6290-6294.

7. H. Huang, S. Zhou, C. Yu, H. Huang, J. Zhao, L. Dai, J. Qiu, Rapid and energy-

efficient microwave pyrolysis for high-yield production of highly-active bifunctional electrocatalysts for water splitting, Energy Environ. Sci., 2020, **13**, 545-553.

8. J. Luo, J.-H. Im, M.T. Mayer, M. Schreier, M.K. Nazeeruddin, N.-G. Park, S.D. Tilley, H.J. Fan, M. Grätzel, Water photolysis at 12.3% efficiency via perovskite photovoltaics and Earth-abundant catalysts, Sci., 2014, **345**, 1593-1596.

9. M. Ledendecker, S. Krick Calderón, C. Papp, H.P. Steinrück, M. Antonietti, M. Shalom, The synthesis of nanostructured Ni_5P_4 films and their use as a non-noble bifunctional electrocatalyst for full water splitting, Angew. Chem. Int. Ed., 2015, **54**, 12361-12365.

10. L.-L. Feng, G. Yu, Y. Wu, G.-D. Li, H. Li, Y. Sun, T. Asefa, W. Chen, X. Zou, High-index faceted Ni_3S_2 nanosheet arrays as highly active and ultrastable electrocatalysts for water splitting, J. Am. Chem. Soc., 2015, **137**, 14023-14026.